Deep and tapered silicon photonic crystals for achieving anti-reflection and enhanced absorption

Yung-Jr Hung[1]*, San-Liang Lee[1], and Larry A. Coldren[2]

[1]Dept. of Electronic Engineering and Intelligent Building Research Center, National Taiwan University of Science and Technology, No. 43, Sec.4, Keelung Rd., Taipei, 106, Taiwan
[2]Department of Electrical and Computer Engineering, University of California at Santa Barbara, Santa Barbara, CA, 93117, USA
*D9502307@mail.ntust.edu.tw

Abstract: Tapered silicon photonic crystals (PhCs) with smooth sidewalls are realized using a novel single-step deep reactive ion etching. The PhCs can significantly reduce the surface reflection over the wavelength range between the ultra-violet and near-infrared regions. From the measurements using a spectrophotometer and an angle-variable spectroscopic ellipsometer, the sub-wavelength periodic structure can provide a broad and angular-independent antireflective window in the visible region for the TE-polarized light. The PhCs with tapered rods can further reduce the reflection due to a gradually changed effective index. On the other hand, strong optical resonances for TM-mode can be found in this structure, which is mainly due to the existence of full photonic bandgaps inside the material. Such resonance can enhance the optical absorption inside the silicon PhCs due to its increased optical paths. With the help of both antireflective and absorption-enhanced characteristics in this structure, the PhCs can be used for various applications.

©2010 Optical Society of America

OCIS codes: (050.5298) Photonic crystals; (160.4760) Optical properties ; (220.4241) Nanostructure fabrication

References and links

1. H. Benisty, J.-M. Lourtioz, A. Chelnokov, S. Combrie, and X. Checoury, "Recent advances toward optical devices in semiconductor-based photonic crystals," Proc. IEEE **94**(5), 997–1023 (2006).
2. A. David, H. Benisty, and C. Weisbuch, "Optimization of light-diffracting photonic-crystals for high extraction efficiency LEDs," J. Display Technol. **3**(2), 133–148 (2007).
3. I. D. Block, L. L. Chan, and B. T. Cunningham, "Photonic crystal optical biosensor incorporating structured low-index porous dielectric," Sens. Actuators B Chem. **120**(1), 187–193 (2006).
4. D.-H. Ko, J. R. Tumbleston, L. Zhang, S. Williams, J. M. DeSimone, R. Lopez, and E. T. Samulski, "Photonic crystal geometry for organic solar cells," Nano Lett. **9**(7), 2742–2746 (2009).
5. Z. Fan, D. J. Ruebusch, A. A. Rathore, R. Kapadia, O. Ergen, P. W. Leu, and A. Javey, "Challenges and prospects of nanopillar-based solar cells," Nano Res. **2**(11), 829–843 (2009).
6. J. Zhu, Z. Yu, G. F. Burkhard, C.-M. Hsu, S. T. Connor, Y. Xu, Q. Wang, M. McGehee, S. Fan, and Y. Cui, "Optical absorption enhancement in amorphous silicon nanowire and nanocone arrays," Nano Lett. **9**(1), 279–282 (2009).
7. E. B. Grann, M. G. Varga, and D. A. Pommet, "Optimal design for antireflective tapered two-dimensional subwavelength grating structures," J. Opt. Soc. Am. A **12**(2), 333–339 (1995).
8. S.-I. Inoue, S. Yokoyama, and Y. Aoyagi, "Direct determination of photonic band structure for waveguiding modes in two-dimensional photonic crystals," Opt. Express **16**(4), 2461–2468 (2008).
9. V. Astratov, D. Whittaker, I. Culshaw, R. Stevenson, M. Skolnick, T. Krauss, and R. De La Rue, "Photonic band-structure effects in the reflectivity of periodically patterned waveguides," Phys. Rev. B **60**(24), 16255–16258 (1999).
10. M. Galli, M. Agio, L. Andreani, M. Belotti, G. Guizzetti, F. Marabelli, M. Patrini, P. Bettotti, L. Dal Negro, Z. Gaburro, L. Pavesi, A. Lui, and P. Bellutti, "Spectroscopy of photonic bands in macroporous silicon photonic crystals," Phys. Rev. B **65**(11), 113111 (2002).
11. C. I. Hsieh, H. L. Chen, W. C. Chao, and F. H. Ko, "Optical properties of two-dimensional photonic-bandgap crystals characterized by spectral ellipsometry," Microelectron. Eng. **73–74**, 920–926 (2004).

#123269 - $15.00 USD Received 25 Jan 2010; revised 12 Mar 2010; accepted 12 Mar 2010; published 17 Mar 2010

12. C.-H. Lin, H.-L. Chen, W.-C. Chao, C.-I. Hsieh, and W.-H. Chang, "Optical characterization of two-dimensional photonic crystals based on spectroscopic ellipsometry with rigorous coupled-wave analysis," Microelectron. Eng. **83**(4-9), 1798–1804 (2006).
13. C.-W. Kuo, J.-Y. Shiu, and P. Chen, "Size- and shape-controlled fabrication of large-area periodic nanopillar arrays," Chem. Mater. **15**(15), 2917–2920 (2003).
14. C.-W. Kuo, J.-Y. Shiu, P. Chen, and G. A. Somorjai, "Fabrication of size-tunable large-area periodic silicon nanopillar arrays with sub-10nm resolution," J. Phys. Chem. B **107**(37), 9950–9953 (2003).
15. Y.-F. Chang, Q.-R. Chou, J.-Y. Lin, and C.-H. Lee, "Fabrication of high-aspect-ratio silicon nanopillar arrays with the conventional reactive ion etching technique," Appl. Phys., A Mater. Sci. Process. **86**(2), 193–196 (2006).
16. Z. Yu, H. Gao, W. Wu, H. Ge, and S. Y. Chou, "Fabrication of large area subwavelength antireflection structures on Si using trilayer resist nanoimprint lithography and liftoff," J. Vac. Sci. Technol. B **21**(6), 2874–2877 (2003).
17. A. A. Ayón, R. Braff, C. C. Lin, H. H. Sawin, and M. A. Schmidt, "Characterization of a time multiplexed inductively coupled plasma etcher," J. Electrochem. Soc. **146**(1), 339–349 (1999).
18. X. Wang, W. Zeng, G. Lu, O. L. Russo, and E. Eisenbraun, "High aspect ratio Bosch etching of sub-0.25 μm trenches for hyperintegration applications," J. Vac. Sci. Technol. B **25**(4), 1376–1381 (2007).
19. C.-H. Choi, and C.-J. Kim, "Fabrication of a dense array of tall nanostructures over a large sample area with sidewall profile and tip sharpness control," Nanotechnology **17**(21), 5326–5333 (2006).
20. K. J. Morton, G. Nieberg, S. Bai, and S. Y. Chou, "Wafer-scale patterning of sub-40 nm diameter and high aspect ratio (>50:1) silicon pillar arrays by nanoimprint and etching," Nanotechnology **19**(34), 345301 (2008).
21. Y.-J. Hung, S.-L. Lee, and Y.-T. Pan, "Holographic realization of two-dimensional photonic crystal structures on silicon substrates," *Integrated Photonics and Nanophotonics Research and Applications (IPNRA'09)*, paper IWD5, Honolulu, Hawaii, USA (2009).
22. Y.-J. Hung, S.-L. Lee, and Y.-T. Pan, "Photonic bandgap analysis of photonic crystal slabs with elliptical holes and their formation with laser holography," J. Opt. **12**(1), 015102 (2010).
23. J. D. Joannapolous, R. D. Meade, and J. N. Winn, "Photonic crystals – molding the flow of light," (Princeton University Press, 1995)
24. S. H. Zaidi, D. S. Ruby, and J. M. Gee, "Characterization of random reactive ion etched-textured silicon soar cells," IEEE Trans. Electron. Dev. **48**(6), 1200–1206 (2001).

1. Introduction

Two-dimensional photonic crystals (2D PhCs) have been extensively studied as the building blocks to realize functional devices for optical networking [1], image display [2], bio-medical sensing [3], and photovoltaic applications [4]. The artificial periodic structures can be used to control the behavior of photons for its photonic bandgap (PBG) and/or light diffraction properties. Recently, as an emerging field, disordered nanopillar arrays are used to improve the efficiency of solar cells through its reduced optical reflection, enhanced absorption and enhanced carrier collection efficiency [5,6]. Tapering of nanopillars could further improve the antireflection and enhanced absorption properties [6,7]. With the help of ordered nanopillars, optical absorption can also be enhanced through multiple excitation resonances [4]. However, to develop a rapid, large-area and high-resolution fabrication scheme for realizing tapered and highly-ordered 2D nanopillars is a challenge.

In this work, we develop a simple technique for directly transferring holographically generated photoresist (PR) patterns into silicon by using a novel single-step deep reactive ion etching (SDRIE) technique. This technique can realize 2D silicon photonic crystals with a high aspect ratio, good uniformity and a tapered sidewall profile without scalloping. The resultant PhC samples are then characterized by using a spectrophotometer and an angle-variable spectroscopic ellipsometer [8–12]. Reflection spectra of this PhC structure under different incident angles and polarizations are measured for observing its antireflection and optical resonant effect. Optical resonance is mainly due to the existence of PBG inside this material. A spectroscopic ellipsometer is also used for further verifying this unique PBG phenomenon. Analysis of the PhC structure with rigorous coupled-wave analysis (RCWA) method, taking the dispersion and absorption of materials into account, is used for verifying the experimental data. It is found that such resonance will enhance the absorption inside the pillars, thus can be potentially used for PhC-based photovoltaic devices.

#123269 - $15.00 USD Received 25 Jan 2010; revised 12 Mar 2010; accepted 12 Mar 2010; published 17 Mar 2010

2. Sample preparation

Synthesis of silicon nanopillar arrays has been investigated in the literatures using various patterning and etching techniques [13–15]. Fabrication of sub-wavelength antireflective structures with tapered sidewall profile was also studied [16]. However, most of them require a metal hard mask formed mostly by lift-off process for the following deep etching. This additional lift-off step will degrade the resolution of the patterned profile and increase process complexity. Deep reactive ion etching (DRIE) can be used for micro-electro mechanical systems (MEMS) and micro-fluidic device fabrication. Multiple-cycles of the cyclic Bosch process enable anisotropic etching of silicon with high mask selectivity (>200:1 for silicon oxide and >75:1 for photoresist) and high etching rate (several µm per min) [17]. However, this technique is not suitable for etching nanostructures due to its scalloping of the sidewalls (the peak-to-valley height is typically the scale of around several hundred nanometers). Recently, with the development of this technology, X. Wang et al. have applied Bosch etching to realize submicron trenches [18] while C.-H. Choi et al. have shown the possibility to control the sidewall profile of nanostructure array by tuning the parameters of Bosch process [19]. More recently K. J. Morton et al. have demonstrated high-aspect-ratio pillar arrays with optimized Bosch conditions and the scalloping of the sidewalls has been minimized to around 10 nm [20]. Nevertheless, due to the cyclic etching/deposition nature of Bosch process, we can still see the periodic "ripples" on the sidewalls of the best pillars. The scalloping effect will become serious for deeper pillar arrays. To prepare a photonic crystal sample for anti-reflection and/or enhanced absorption, it is desired to avoid the scalloping effect during DRIE process.

In this work, 2D periodic templates with a hexagonal lattice of elliptical geometry are realized using the holographic lithography with a double exposure and a 60-degree sample rotation over a large area [21]. The purpose of using the hexagonal lattice is to obtain a broader PBG area; even though its geometry is elliptical [22]. With an optimized process procedure, the width of the resultant patterns can be adjusted and fine tuned by controlling the total exposure energy and development time [21]. A Plamsa-Therm 770 SLR series system with a loadlock is used to transfer PhC patterns directly from the PR mask into silicon. The system allows to independently controlling the plasma density and ion energy. It is dedicated to deep etching in silicon by using the cyclic Bosch process. However, due to the alternative passivation and etching nature of the Bosch process, scalloping of the sidewalls appears in the etched patterns. We developed a SDRIE process with a controlled mixture of $Ar/SF_6/C_4F_8$ gas to attain smooth and controllable sidewalls while simultaneously keeping the advantages of high etching rate (~222 nm/min) and high mask selectivity (~85:1). Figure 1(a) shows the comparison of process flow between standard Bosch process and SDRIE process. Polymer deposition for protecting lateral sidewalls and deep silicon etching proceed simultaneously in SDRIE process. The slope of etched sidewall profile can be easily controlled by engineering the composition of gas mixture.

Figure 1(b) shows the overall process for fabricating silicon photonic crystals. A silicon substrate is cleaned and an antireflection coating (ARC) layer (XHRiC-11 ARC from Brewer Science) is deposited by spin-coating at 3000 rpm for 30 seconds. After pre-baking ARC layer on a hot plate at 165 degrees for 60 seconds, a positive PR layer is deposited at 3000 rpm for 30 seconds and soft baked at 90 degrees for 90 seconds. The sample is then transferred to the laser holography system and exposed twice with a dose of 30.24 mJ/cm^2 for each exposure. Following the double-exposure, a post-exposure bake is performed on a hot plate at 115 degrees for 120 seconds to further reduce the standing-wave effect in the resist sidewalls. The sample is then developed to attain a periodic template. Transferring the PR patterns into bottom ARC layer is then carried out by anisotropic O_2 plasma using a conventional reactive ion etching machine with an O_2 flow of 10 sccm, a pressure of 10 mTorr, and a RF voltage of 250V. Figure 2(a) shows the SEM photos of the 2D PR/ARC templates. The height, lattice constant, and ellipticity (ratio between major- and minor-axis of

#123269 - $15.00 USD Received 25 Jan 2010; revised 12 Mar 2010; accepted 12 Mar 2010; published 17 Mar 2010
(C) 2010 OSA

ellipse) of the resultant patterns are around 250 nm, 375 nm and 1.41, respectively. Samples with a hexagonal lattice and high uniformity are demonstrated over a large area.

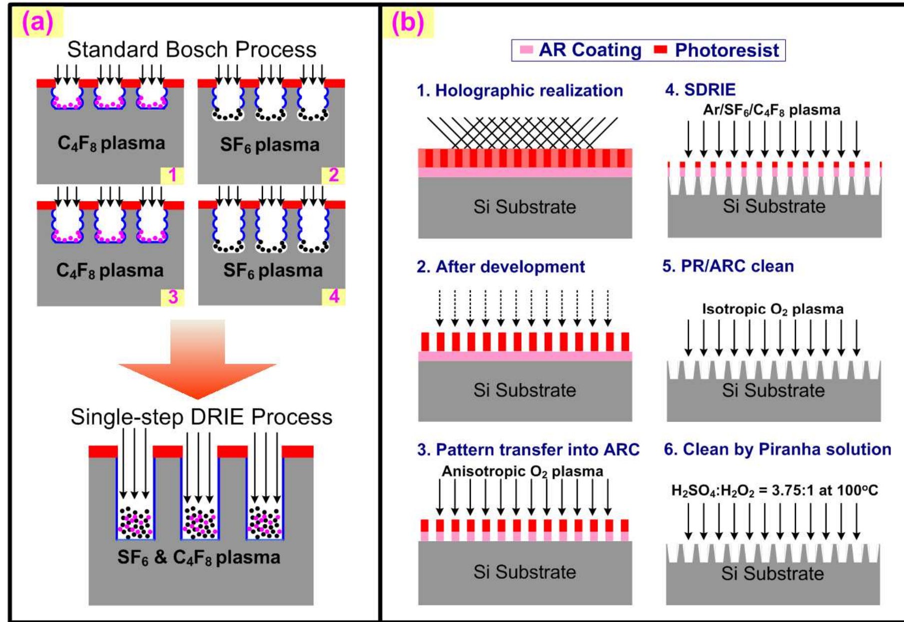

Fig. 1. (a) comparison of process flow between conventional Bosch process and SDRIE process (b) fabrication procedures of silicon photonic crystals by holographic lithography and SDRIE

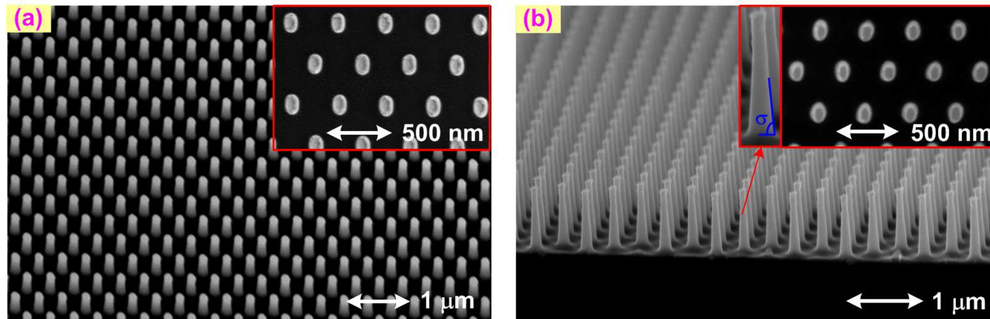

Fig. 2. SEM photos of (a) resultant 2D PR/ARC templates and (b) resultant 2D silicon photonic crystals

The substrate is then etched by SDRIE using the PR/ARC pattern as a hard mask. For the mechanism of this reactive gas mixture, isotropic etching of the silicon is carried out by SF_6/Ar plasma while sidewall protection is carried out by plasma deposition of C_4F_8. Balance between etching and deposition is the key to attain patterns with vertical sidewalls. However, in this work, less SF_6 (26 sccm) and more C_4F_8 (54 sccm) is used to obtain tapered nanostructures. For comparison, a non-tapered silicon photonic crystal sample is fabricated by using similar process conditions but with 28-sccm SF_6 and 52-sccm C_4F_8 flow rate. For both etching recipes, the pressure in the chamber is set to be 19 mTorr. The power of the RIE generator and ICP are fixed at 9 W and 850 W, respectively. Selectivity between silicon and PR/ARC mask is about 85:1 for both etching recipes. After dry etching, the remaining PR/ARC is removed by isotropic O_2 plasma with an O_2 flow of 20 sccm, a pressure of 80

#123269 - $15.00 USD Received 25 Jan 2010; revised 12 Mar 2010; accepted 12 Mar 2010; published 17 Mar 2010
(C) 2010 OSA

mTorr, and a RF voltage of 250V. Finally, the substrate is cleaned with a Piranha solution (H_2SO_4:H_2O_2 = 3.75:1 by volume with a lifted temperature of 100 degree Celsius).

The tapered silicon photonic crystal is 800 nm tall with a slope (the tangent of σ, the angle of slope) of 15.4, an average ellipticity of 1.6228, and a filling factor (averaged radius-to-period ratio) of 0.146, as shown in Fig. 2(b). The non-tapered reference sample is 850 nm tall with vertical sidewalls of which the slope is about 143, corresponding to an angle σ of about 89.6°. It has an average ellipticity of 1.63 and a filling factor of 0.167. The resultant PhC sample is highly uniform over the entire sample area, around 1 cm^2, as shown in Fig. 4(a). The size of the PhC patterns will be limited by the exposed area of the holographic setup.

3. Optical characterization

The optical properties of the etched samples are characterized by a spectrophotometer and an angle-variable spectroscopic ellipsometer. Figure 3(b) shows the photograph of the angle-adjustable (30° to 90°) spectroscopic ellipsometer which consists of a xenon lamp light source, a monochrometor, a beam chopper, a sample stage with a goniometer base, and a detector with a rotating analyzer. All components are connected to a control module which can be controlled via a computer. In this setup, reflection spectra under different incident angles can be measured by changing the angle θ of this system. Reflection spectra along the symmetric points of hexagonal silicon PhCs can also be obtained by adjusting the sample orientation ϕ. In this experiment, the light beam that is polarized parallel (perpendicular) to the plane of incidence, is named TM (TE) polarization, as indicated in Fig. 2(b). In contrast, TE_{phc} (TM_{phc}) refers to the direction of optical resonance of the PhCs that is parallel to the pillars (silicon substrate).

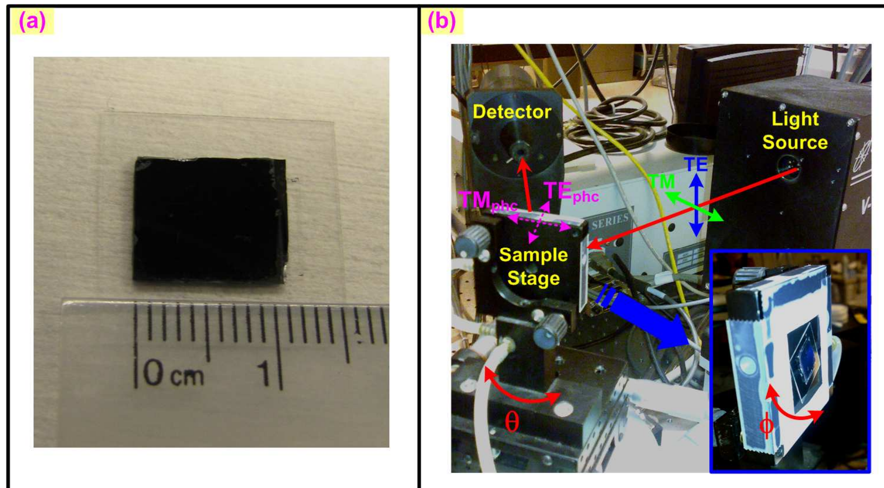

Fig. 3. (a) photo of the resultant PhC sample (b) photograph of the testing setup

Figure 4(a) shows the close-to-normal (8-degree) incident optical reflection spectrum of bare silicon, 2D PR/ARC templates on silicon, and tapered and non-tapered silicon photonic crystals that are measured by using a spectrophotometer with an un-polarized light source. Lower reflectivity of 2D PR/ARC templates is due to its lower effective index which serves as a buffer layer between air and silicon substrate. Dips at around 365 nm of wavelength as well as in the ultraviolet (UV) region are due to the absorption characteristic of the ARC. The tapered silicon photonic crystals has a much lower reflectivity than the bare silicon over a wide wavelength range due to its deeper sub-wavelength structure and gradually changed effective index between air and silicon. Slight optical resonant effect can be seen at the wavelengths of 1200 nm, 550 nm and UV region in Fig. 4(a). By combining those effects, the

#123269 - $15.00 USD Received 25 Jan 2010; revised 12 Mar 2010; accepted 12 Mar 2010; published 17 Mar 2010
(C) 2010 OSA

overall reflectivity of this tapered nanostructure under 8-degree incidence is below 10% in the entire UV-to-visible region and is only around 2% in the wavelengths between 500 nm and 600 nm. On the contrary, a narrower AR window and higher minimum reflectivity (~5%) is observed for the non-tapered nanostructure. This verifies that the use of tapered rods can reduce the reflection and enlarge the bandwidth of AR window due to its gradually changed effective index. The reflection spectrum of non-tapered PhCs is slightly red-shifted because of its taller and wider pillar structure.

Figure 4(b) shows the PBG diagram of the silicon PhC structure, calculated by using the 2D plane wave expansion method (2D-PWE) [23]. Due to the noncircular geometry of the silicon photonic crystals, the use of new directions to represent one quarter of the Brillouin zone (Γ-K-M-Γ-K-M'-Γ-K'-M'-Γ) is necessary for PBG calculation as well as for its characterization [22]. The broad TE_{phc}-mode PBG area shown in Fig. 4(b) indicates the existence of full PBGs in this structure. To investigate the optical resonance in this silicon PhC structure, angular dependent zeroth-order reflection spectra along these symmetry points are measured by using the testing setup shown in Fig. 3(b).

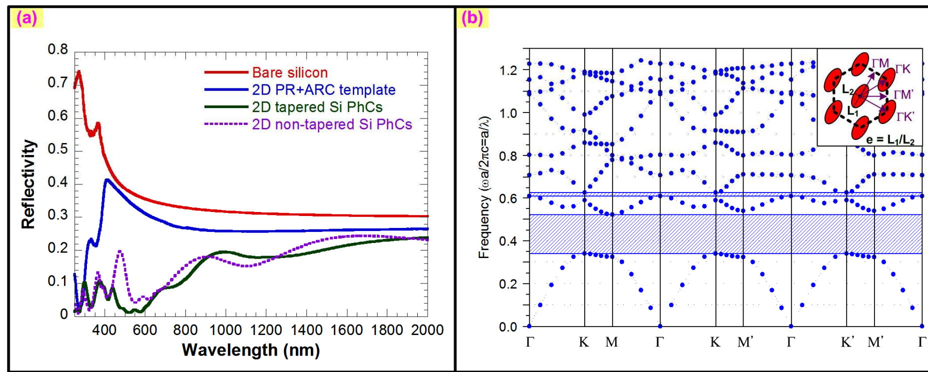

Fig. 4. (a) Measured optical reflection spectrum of bare silicon, 2D PR/ARC templates on silicon, tapered and non-tapered silicon PhCs with close-to-normal (8-degree) incidence (b) Calculated TE_{phc}-mode PBG diagram of our silicon photonic crystals

Figure 5 shows the measured angled-incident reflection spectra along symmetry points of the hexagonal silicon PhCs for the TM- and TE-polarizations. Reflection spectra of bare silicon under the same experimental conditions are also measured for comparison. Noise in the reflection spectra at the wavelength ranges between 900 nm and 1000 nm is due to the turnover of the monochromator. The reflection of bare silicon for TE-polarization increases as the incident angle rises, while the reflection for the TM-polarized light reaches minimum at the Brewster angle (about 70 degrees). Once a tapered PhC sample is employed, the incident light will couple into the local resonance modes (TE_{phc} and TM_{phc}) of PhCs. For oblique incidence with TE-polarized light, the light will be only coupled into the TM_{phc} resonance of PhCs. Only slight resonance is found from the corresponding reflection spectra. This is partly due to the lack of full PBG for TM_{phc} mode in the nanopillar structure. Furthermore, the tapered silicon PhC has a gradually changed effective index and serves as a good buffer layer between air and silicon substrate for the TE-polarized light. This results in a broad and angular-independent antireflective window between 400 and 700 nm of wavelength. The measured reflectivity at 40- and 70-degree of incident angles in this antireflective window is below 1% and 3%, respectively. By comparing to the large reflectivity of bare silicon (around 45% and 70% at 40- and 70-degree of incident angle) for the same polarization, the tapered PhC can transmit more TE-polarized light into the silicon in both normal and angled incidence.

For TM-polarized light, the oblique incidence of light will be coupled into both TE_{phc} and TM_{phc} resonance of PhCs. The coupling efficiency of each mode depends on the incident angle. At a small incident angle, more light is coupled to the TM_{phc} mode, so the reflection

#123269 - $15.00 USD Received 25 Jan 2010; revised 12 Mar 2010; accepted 12 Mar 2010; published 17 Mar 2010
(C) 2010 OSA

spectrum is somewhat similar to that of a TE-polarized light. In contrast, more light is coupled into the TE_{phc} mode as the incident angle is larger. From Fig. 5(a), resonances at the wavelengths around 1100 nm and 650 nm as well as in the UV region are observed in the TM-mode reflection spectra for an incident angle of 40 degrees. The resonance becomes stronger with an incident angle of 70 degree because more light is coupled into the TE_{phc} mode. Similar resonance phenomenon is found along all symmetric points of this PhC structure. The resonance will help to trap the light inside the PhC structure and thus enhance the absorption.

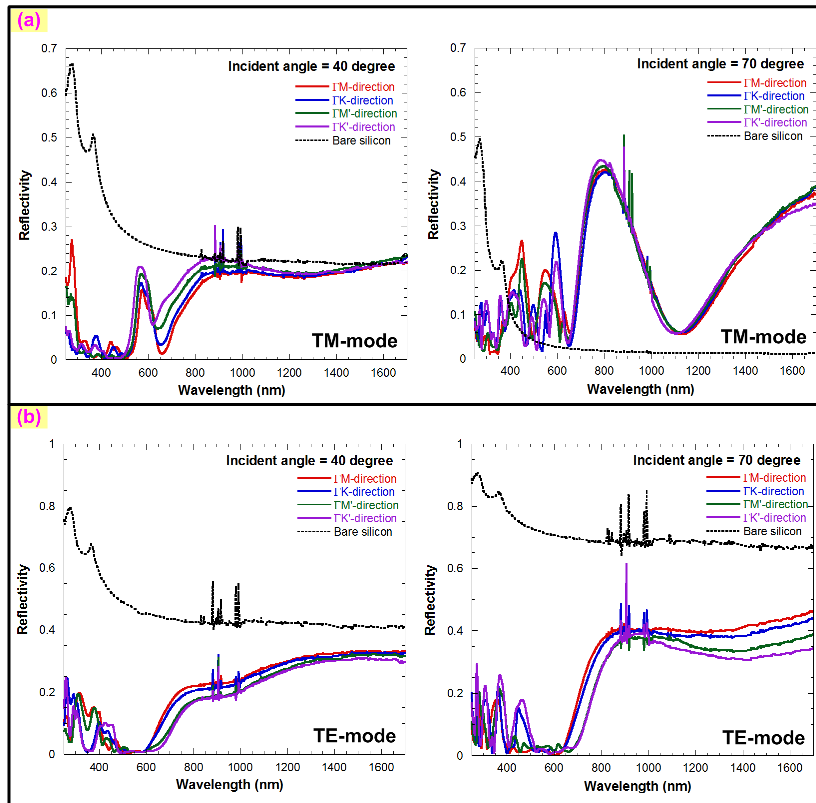

Fig. 5. Measured 40- and 70-degree angled-incident reflection spectra along symmetry points of hexagonal silicon PhCs for (a) TM- and (b) TE-polarization

Figure 6 shows the 2D contour maps of the measured reflection spectra of tapered silicon photonic crystals along ΓM-direction under different incident angles. At small incident angle, weaker resonance and low reflection is observed for both the TE- and TM-modes over the shorter-wavelength range.

#123269 - $15.00 USD Received 25 Jan 2010; revised 12 Mar 2010; accepted 12 Mar 2010; published 17 Mar 2010
(C) 2010 OSA

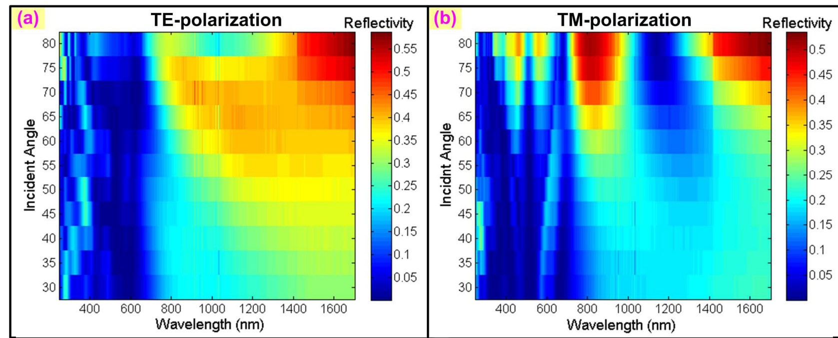

Fig. 6. 2D contour maps of measured reflection spectra of tapered silicon photonic crystals along ΓM-direction under different incident angles for (a) TE- and (b) TM-polarization incidence

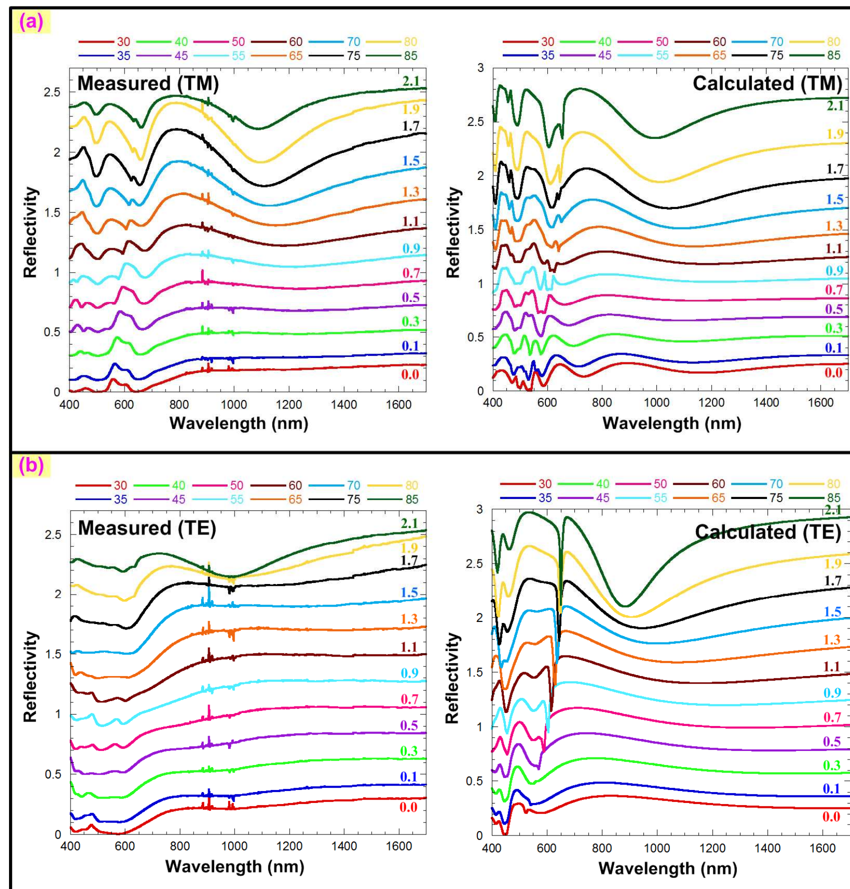

Fig. 7. Measured and calculated reflection spectra at different incident angles along the ΓM-direction of hexagonal silicon PhCs for (a) TM- and (b) TE- polarization. For clarify, the offset of curves are shown inside the plots.

The TM resonance in this structure is mainly due to the existence of PBG which causes dips in the angular reflection spectra [10]. In order to verify this effect, the PBG location is calculated by solving the Maxwell equation with rigorous coupled-wave analysis (RCWA) method. This method can account for both dispersion and absorption of materials as well as the finite-height of the fabricated silicon PhCs. The geometry of the silicon PhCs for RCWA

#123269 - $15.00 USD Received 25 Jan 2010; revised 12 Mar 2010; accepted 12 Mar 2010; published 17 Mar 2010
(C) 2010 OSA

simulation is set according to the real structure parameters described in Section 2 except that vertical sidewalls are assumed in the simulation model.

Figure 7 compares the measured and calculated reflection spectra under different incident angles and polarizations along the ΓM-direction of the hexagonal silicon PhCs. For clarity, the curves are offset with the value shown inside the plots. Similar behavior is found along the other symmetric points of this structure. From the dips in the measured angular reflection spectra, as shown in Fig. 7(a), the PBGs locate at the wavelengths around 650 nm and 1100 nm [10]. There is a good agreement between the experimental and calculated spectra, although measured reflection spectra show weaker resonances, especially for the TE-polarization. This is due to the tapered sidewall of the real structure which reduces the resonant effect. According to the calculated distribution of electric field in the reflection plane of this structure, the electric field for the TE_{phc} resonance confines inside the pillars while that for the TM_{phc} resonance falls between the pillars. The TM_{phc} resonance will be greatly reduced in a tapered structure. Thus for oblique TE-mode incidence, optical resonance effect is greatly reduced since all of the light will couple into TM_{phc} resonance. On the other hand, the antireflective effect due to the gradually changed effective index of this structure is dominant for the TE incidence and provides a broad and relatively angular-independent antireflective window in the visible region.

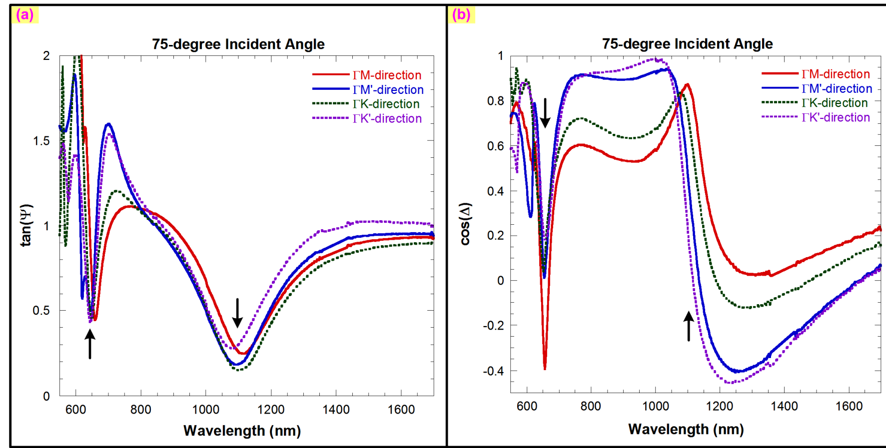

Fig. 8. Measured spectra of PBG ellipsometry parameters (a) tan(ψ) and (b) cos(Δ) along symmetry points of the hexagonal silicon PhCs. Arrows shown in the plots indicate the PBG positions.

We also use the spectral ellipsometry for characterizing the PBG of PhCs [11,12]. The ellipsometry measures two of the four Stokes parameters, which are denoted by ψ and Δ. The polarization state of the light incident upon the sample can be decomposed into a TE and a TM component. The reflection of the TE and TM components are denoted by R_{TE} and R_{TM}, respectively. The ellipsometry measures the ratio of R_{TE} and R_{TM}, $\rho = R_{TM} / R_{TE} = \tan(\Psi) e^{i\Delta}$. Here, tan(ψ) is the amplitude ratio and cos(Δ) is the phase difference through the material-light interaction. The measured ellipsometry parameters along the symmetry points of hexagonal silicon PhCs are shown in Fig. 8. For oblique incidence, the reflection of different polarized light would manifest differently in their corresponding spectra. The TE_{phc} bandgap leads to higher out-of-plane diffraction for the TM-polarized light [10], resulting in lower reflection and thus lower tan(ψ) value. Meanwhile, the TM-polarized light would increase its optical paths and corresponding lower cos(Δ) value [11]. The reflection caused by the TE_{phc}-mode PBG would then appear as a dip and a steep slope in the tan(ψ) and cos(Δ) spectra, respectively [11,12]. We indeed find similar phenomenon at the wavelengths of 650 nm and 1100 nm along the symmetry points, as indicated by the arrows in Fig. 8, verifying the existence of full TM PBGs inside the PhCs.

#123269 - $15.00 USD Received 25 Jan 2010; revised 12 Mar 2010; accepted 12 Mar 2010; published 17 Mar 2010
(C) 2010 OSA

One of the potential applications for tapered PhC materials is the photovoltaic devices. The angle dependence of the reflectivity can affect the energy conversion of fixed outdoor solar-cell panels, because the angle of solar irradiation varies during a day. The use of surface random textures or AR coatings can also reduce the reflectivity of the Si surface, but their AR effects have strong angle dependence, which may result in a large variation of the output power for solar cells irradiated at oblique angles. With the proposed tapered PhCs, antireflection can be obtained for both TE- and TM-polarized light with relative small-angled incidence (0-45 degree) since most of light will couple into the TM_{phc} mode of PhC. The broadband and angular-independent AR window is beneficial for coupling the input energy to solar cells. Absorption enhancement will become dominant for TM-polarized light with a large incident angle (> 45 degree) since more light will couple into TE_{phc} mode of PhC and cause optical resonance. The optical resonance, which increases the total optical paths, is vital for increasing light absorption at longer wavelengths where the absorption coefficient is small, especially for thin Si-film substrates. Meanwhile, the AR effect can still be attained for the TE-polarized light with a large incident angle. One of the possible device architectures that utilize both the antireflection and absorption effects of PhCs is to employ P-N junction inside the pillars such that the light will always touch the active layer and contribute to the photocurrent. Though the dry-etched surface may have higher surface recombination velocities and plasma-induced damage, surface passivation and/or controlled wet-chemical damage removal etches can be used to reduce the defects [24].

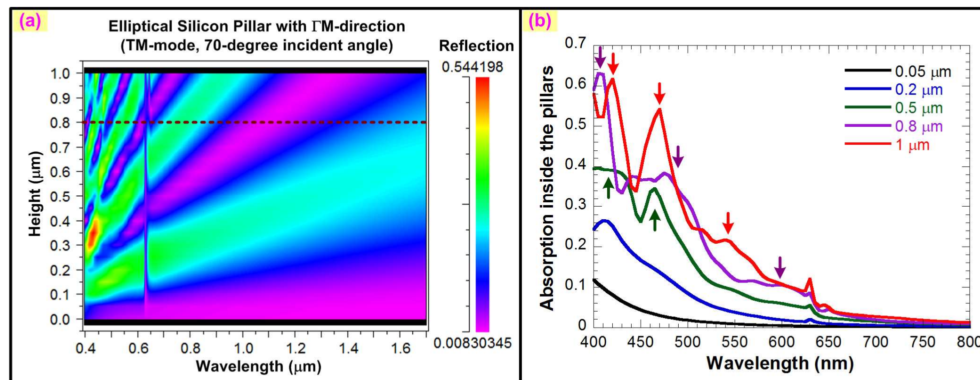

Fig. 9. Calculated 70-degree angled-incident (a) reflection and (b) absorption spectra of silicon PhCs in the TM polarization for different pillar heights. The lattice constant of PhC pillars is set to 375 nm.

4. Discussion

We further investigate the effects of pillar height on the resonance phenomenon of this silicon PhCs by using the RCWA method. The pillars are still assumed to have vertical sidewalls. Figure 9 shows the calculated reflection and absorption spectra versus pillar height for the TM polarization at an incident angle of 70 degrees. There is a dip at around 640 nm of wavelength throughout all reflection spectra in Fig. 9(a), thus enhancing the absorption as shown in Fig. 9(b). This is probably due to the multiple excitation resonance which was reported recently [4]. There are several dips in the reflection spectra that strongly depend on the pillar height. These are caused by the existence of PBG. The dash line shown in Fig. 9(a) indicates the case for the fabricated 800-nm tall PhC structures. The overlap of dips that are caused by the multiple excitation resonance and PBGs are found in Fig. 9(a). The enhancement on the optical absorption is stronger for taller pillars, especially for the wavelengths within the PBGs. Arrows shown in Fig. 9(b) indicate the locations of PBGs. For the case of 0.8 μm tall PhC pillars, optical absorption at 500-600 nm wavelength bands is enhanced. Since the location of dips in the measured reflection spectra shown in Fig. 7(a) are

#123269 - $15.00 USD Received 25 Jan 2010; revised 12 Mar 2010; accepted 12 Mar 2010; published 17 Mar 2010
(C) 2010 OSA

similar to the calculated ones, we can expect that the enhanced absorption in the fabricated PhC pillars also follows the calculated curve shown in Fig. 9(b).

Figure 10 shows the calculated reflection and absorption spectra against the lattice constant for the TM polarization at an incident angle of 70 degrees. It can be found from Fig. 10(a) that the multiple excitation resonance depends strongly on the lattice constant of the PhC structure. On the contrary, the PBG position can be fine tuned by simply changing the lattice constant of the PhCs. The PBG moves toward longer wavelength as we increase the lattice constant of the PhCs, thus red-shifting the enhanced absorption, as shown in Fig. 10(b). Arrows shown in Fig. 10(b) indicate the location of PBGs. However, the PBGs disappear in the UV-to-visible region as the lattice constant of PhCs is larger than 500 nm. Therefore, PhCs with a lattice constant of less than 450 nm are considered to be a better choice for enhancing the optical absorption over the visible wavelengths.

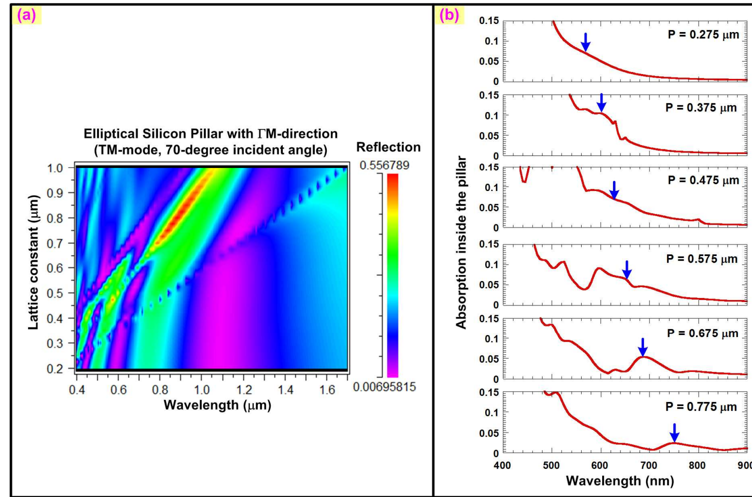

Fig. 10. The variation of the calculated (a) reflection and (b) absorption spectra of silicon PhCs with the lattice constant (P), along the TM polarization at 70-degree incident angle. The height of PhC pillars is set to 800 nm.

5. Conclusion

We fabricated deep and tapered silicon photonic crystals and demonstrated their anti-reflection and enhanced absorption characteristics. To realize such structures with high resolution and fast process time, we developed a technique to directly transfer the holographic generated PR/ARC patterns into silicon by using a novel SDRIE scheme with a controlled mixture of $Ar/SF_6/C_4F_8$ gas. Tapered and tall (800-nm high) silicon photonic crystals with smooth sidewall surface (no scalloping), an averaged ellipticity of 1.6228, and a filling factor of 0.146 is realized with high uniformity over the entire sample area.

Reflection spectra of this PhC structure under different incident angles and polarizations are measured for observing its optical characteristics. For small incident angles, the PhCs has low reflectivity over the visible wavelengths for both TE and TM modes. The tapered PhC structure that has a gradually changed effective index serves as a good buffer layer between air and silicon, resulting in a broad antireflective window. This effect is especially beneficial for the TE-polarized light, and the antireflective window can be obtained over a large incident angle. On the other hand, strong optical resonances for TM-mode are found in this structure, which is mainly due to the existence of full PBGs inside the material. This PBG phenomenon is further verified by the spectroscopic ellipsometry. Such strong resonance will greatly enhance the optical absorption inside silicon PhCs. According to the RCWA simulation results, enhanced optical absorption is found for taller silicon PhC pillars, especially for the wavelengths within the PBGs, and can be fine tuned by changing the lattice

#123269 - $15.00 USD Received 25 Jan 2010; revised 12 Mar 2010; accepted 12 Mar 2010; published 17 Mar 2010
(C) 2010 OSA

constant of the PhCs. PhCs with a lattice constant of less than 450 nm are considered to be a better choice for enhancing the optical absorption over the visible wavelengths. With the help of both antireflective and absorption-enhanced characteristics in this structure, this PhC material can be used for various applications.

Acknowledgment

We acknowledged Dr. Brian Thibeault for his help in developing SDRIE technique. This work is supported in part by the National Science Council, Taiwan, under grant NSC97-2221-E-011-077-MY3 and NSC97-2917-I-011-103 and by the Ministry of Education, Taiwan under the Top University Program. Part of this work is done in the UCSB nanofabrication facility, part of the NSF funded NNIN network.

#123269 - $15.00 USD Received 25 Jan 2010; revised 12 Mar 2010; accepted 12 Mar 2010; published 17 Mar 2010
(C) 2010 OSA